PAPER • OPEN ACCESS

Analysis of leakage artifacts and their impact on convergence of algebraic reconstruction in multi-contrast magnetic particle imaging

To cite this article: Lina Nawwas *et al* 2024 *Phys. Med. Biol.* **69** 215002

IOP Publishing Phys. Med. Biol. 69 (2024) 215002 https://doi.org/10.1088/1361-6560/ad7e77

Physics in Medicine & Biology

IPEM Institute of Physics and Engineering in Medicine

OPEN ACCESS

RECEIVED
16 May 2024

REVISED
30 August 2024

ACCEPTED FOR PUBLICATION
23 September 2024

PUBLISHED
11 October 2024

PAPER

Analysis of leakage artifacts and their impact on convergence of algebraic reconstruction in multi-contrast magnetic particle imaging

Lina Nawwas[1,2,*], **Martin Möddel**[1,2] and **Tobias Knopp**[1,2]

[1] Institute for Biomedical Imaging, University Medical Center Hamburg-Eppendorf, Hamburg, Germany
[2] Institute for Biomedical Imaging, Hamburg University of Technology, Hamburg, Germany
[*] Author to whom any correspondence should be addressed.

E-mail: l.nawwas@uke.de

Keywords: magnetic particle imaging, multi-contrast magnetic particle imaging, reconstruction artifacts, channel leakage

Abstract

Objective. Magnetic particle imaging (MPI) is a tracer-based medical imaging modality with great potential due to its high sensitivity, high spatiotemporal resolution, and ability to quantify the tracer concentration. Image reconstruction in MPI is an ill-posed problem, which the use of regularization methods can address. Multi-contrast MPI reconstructs the signal from different tracer materials or environments separately, resulting in multi-channel images that enable quantification of, for example, temperature or viscosity. Single- and multi-contrast MPI reconstructions produce different kinds of artifacts. The objective of this work is threefold: first, to present the concept of multi-contrast specific MPI channel leakage artifacts; second, to ascertain the source of these leakage artifacts; and third, to introduce a method for their reduction. *Approach.* A definition for leakage artifacts is established, and a quantification method is proposed. A comprehensive analysis is conducted to establish a connection between the properties of the multi-contrast MPI system matrix and the leakage artifacts. Moreover, a two-step measurement and reconstruction method is introduced to reduce channel leakage artifacts between multi-contrast MPI channels. *Main results.* The severity of these artifacts correlates with the system matrix shape and condition number and depends on the similarity of the corresponding frequency components. Using the proposed two-step method on both semi-simulated and measured data a significant leakage reduction and speed up the convergence of the multi-contrast MPI reconstruction was observed. *Significance.* The multi-contrast system matrix analysis we conducted is essential for understanding the source of the channel leakage artifacts and finding methods to reduce them. Our proposed two-step method is expected to improve the potential for real-time multi-contrast MPI applications.

1. Introduction

Imaging artifacts are generally defined as features that appear in an image but do not exist in the originally imaged object (Barnhart and Steinmetz 1999, Hsieh 2009, Bell *et al* 2018). They are observed for various imaging techniques, such as medical imaging, microscopy, photography, etc. Artifacts can occur for various reasons including hardware, or processing-related problems, equipment limitations, physical restrictions, or model imperfections. Understanding these artifacts and their sources is essential to finding ways to mitigate them effectively.

In medical imaging, the most commonly obtained artifact is image noise and processing-related artifacts (Bell *et al* 2018), which are inherent to every modality, and can be mitigated but never completely eliminated. Knowledge of these artifacts is important as some of them can seriously influence the diagnostic image quality or be confused with another pathology (Triche *et al* 2019). The study and analysis of imaging artifacts and the development of methods to reduce them is an ongoing research focus for all major medical

imaging modalities, see Barrett and Keat (2004), Dietrich *et al* (2008), Shetty *et al* (2011), Boas and Fleischmann (2012), Walz-Flannigan *et al* (2012), Mori *et al* (2013), Budrys *et al* (2018)and the references therein for more details.

Magnetic particle imaging (MPI) is an emerging tomographic medical imaging modality that employs static and dynamic magnetic fields (Gleich and Weizenecker 2005, Knopp and Buzug 2012). It is tracer-based and designed to determine the concentration of magnetic nanoparticles (MNPs). The standard MPI reconstruction approach referred to as single-contrast MPI, recovers the particle distribution from a measurement using a single system function. However, it has been proven that MPI can also recover the particle distribution from multiple tracers simultaneously. This multi-contrast approach uses multiple system functions for reconstruction to separate the signal from different tracers into different channels given a single measurement (Rahmer *et al* 2015). Here, different tracers refer not only to nanoparticles with different internal structures, such as the material they are made of Rahmer *et al* (2015) or their core size (Shasha *et al* 2019) but also to differences induced by changes in the particles' environment, such as temperature (Stehning *et al* 2016) or viscosity (Möddel *et al* 2018).

Although not as well studied or understood, artifacts are present in MPI as in other imaging modalities. In MPI setups, images are obtained by solving a linear ill-posed inverse problem (Grüttner *et al* 2013, Kluth 2018), for which the standard least squares methods are used. In practice, this leads to large variances in the reconstructed images stemming from measurement noise when minimizing the least squares data discrepancy only. Regularization methods are commonly used in MPI to reduce the impact of noise, however, they come at the expense of a bias in the reconstruction results (Brinkmann *et al* 2017, Nawwas *et al* 2021). Bias is mainly a systematic deviation of the reconstruction result from the true data, for example, the commonly used Tikhonov regularization in MPI can produce bias in the form of an over- or under-estimation of the tracer concentration or certain structural artifacts in the reconstructed image. Those artifacts are usually spatially correlated to the reconstructed object and occur as blurring, over-shooting, or over-smoothing. Another typically observed type of artifact is not spatially correlated to the reconstructed object but appears in the reconstructed images in the form of random noisy structures. Artifacts in MPI and methods to handle them have been investigated in some works, for instance, artifacts reduction using overscanning (Weber *et al* 2015), reconstruction quality improvement using frequency selection and weighting (Knopp *et al* 2010) and bias reduction for sparsity promoting regularization (Nawwas *et al* 2021). However, a generalized mathematical model for artifacts in MPI and an in-depth analysis of artifacts in multi-contrast MPI are still missing (Herbst and Franke 2018, Glöckner *et al* 2020).

This paper is the full and extended version of our conference abstracts (Nawwas *et al* 2024a, 2024b). A detailed systematic investigation of the multi-contrast MPI reconstruction artifacts, which we refer to as channel leakage, is conducted. An analysis of the multi-contrast MPI system matrix properties is performed to understand the source of the channel leakage artifacts. The two-step measurement and reconstruction method is discussed in more details to quantify and reduce the leakage between multi-contrast channels. The evaluation of additional data, including semi-simulated and measured data, and the in-depth discussion of the method are also substantial additions to this manuscript.

2. Problem statement

The excitation of the MNPs in MPI results in a signal that can be described by an integral equation, which is linear with respect to the spatial distribution of the MNPs with the so-called system function as the integral kernel. This work considers the MPI system matrix-based image reconstruction approach, which is commonly conducted using the Tikhonov regularization method (Knopp *et al* 2017, Kluth 2018).

The MPI reconstruction is commonly solved using the Tikhonov regularization with the iterative Kaczmarz method. Figure 1 shows reconstruction results using the state-of-the-are approach for single- and multi-contrast simulations to illustrate artifacts in both cases. The formation of the simulations will be introduced in detail in section 4.3. The first column of the figure shows the reconstruction results of a stenosis phantom in a single-contrast MPI simulation using 10 and 50 iterations of the Tikhonov regularized Kaczmarz solver. Regardless of the number of iterations, unstructured artifacts are observed at the top and bottom and an overshooting effect is seen due to the use of Tikhonov regularization. The second and third columns of the figure show the reconstruction results of a multi-contrast MPI simulation consisting of a stenosis and a catheter in the first and second channels, respectively. The first channel of the multi-contrast reconstruction results shows similar artifacts to the ones observed in the single-channel reconstruction, while the second one shows a new type of artifact that is spatially correlated to the object in the first channel. The artifacts are very dominant. Therefore, it is hard to recognize the reconstructed object. However, one can also see that these artifacts are reduced with the number of iterations, which is the reason why often, a much higher number of iterations are used in multi-contrast MPI (Möddel *et al* 2018, 2021, Shasha *et al* 2019).

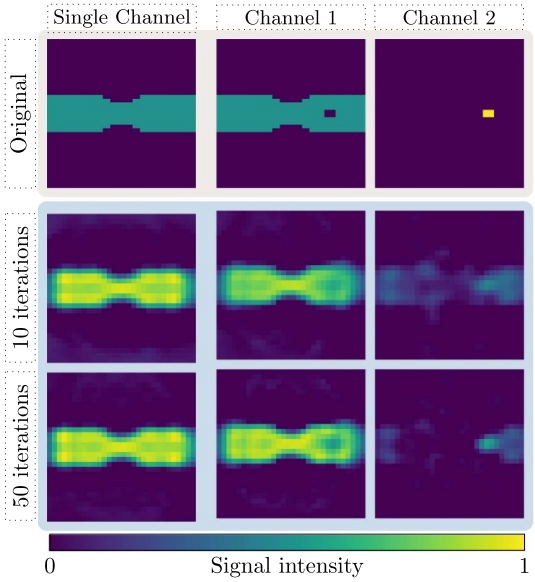

Figure 1. Initial reconstruction results for single- and multi-contrast simulations using the standard Kaczmarz method for a different number of iterations and the same regularization parameter.

3. Theory

This section provides a general theoretical background of single- and multi-contrast MPI, where the single- and multi-contrast reconstruction problems are explained. The effect of the different particle environments or types on the particle magnetization response in multi-contrast MPI is also considered. Then, a generalized model representing the artifact contributions in single- and multi-contrast models is formulated with a special focus on introducing the definition of channel leakage in multi-contrast.

3.1. Multi-contrast MPI problem

In single-contrast MPI, the relation between the particle concentration $\boldsymbol{c} \in \mathbb{R}_+^N$ and the measured signal $\boldsymbol{u} \in \mathbb{C}^M$ in frequency space can be described by a linear system of equations, which can be written in a matrix-vector notation as

$$\boldsymbol{S}\boldsymbol{c} = \boldsymbol{u}, \tag{1}$$

where $\boldsymbol{S} \in \mathbb{C}^{M\times N}$ is the MPI system matrix. The system matrix $\boldsymbol{S}$ describes the relation between the signal response spectrum and the spatial nanoparticle distribution and is obtained by a calibration-based, model-based, hybrid, or compressed-sensing approach in MPI (Knopp *et al* 2017).

Reconstructing the particle concentration $\boldsymbol{c}$ in standard single-contrast MPI is commonly done algebraically by solving the Tikhonov regularized optimization problem (Knopp *et al* 2017, Kluth 2018)

$$\boldsymbol{c}^* = \underset{\boldsymbol{c}\in\mathbb{R}_+^N}{\operatorname{argmin}} \|\boldsymbol{S}\boldsymbol{c} - \boldsymbol{u}\|_2^2 + \lambda\|\boldsymbol{c}\|_2^2, \tag{2}$$

where $\lambda > 0$ is the regularization parameter that is used to control the trade-off between noise and bias.

For multi-contrast MPI, consider a number $\Theta \in \mathbb{N}$ of calibration samples and let $\boldsymbol{S}_i \in \mathbb{C}^{M\times N}, i = 1, 2, \ldots, \Theta$ be the system matrix acquired using the ith sample. Given a measurement $\boldsymbol{u} \in \mathbb{C}^M$, the generalized multi-contrast MPI forward model is formulated as

$$\sum_{i=1}^{\Theta} \boldsymbol{S}_i\boldsymbol{c}_i = \boldsymbol{u}, \tag{3}$$

where $\boldsymbol{c}_i \in \mathbb{R}_+^N$ is the particle concentration corresponding to the ith sample. Concatenating the system matrices $\boldsymbol{S}_i$ and the channels $\boldsymbol{c}_i$ gives us

$$\tilde{\boldsymbol{S}} = \begin{pmatrix} \boldsymbol{S}_1 & \boldsymbol{S}_2 & \ldots & \boldsymbol{S}_\Theta \end{pmatrix} \in \mathbb{C}^{M\times\Theta N}$$

and

$$\tilde{\boldsymbol{c}} = \begin{pmatrix} \boldsymbol{c}_1 \\ \boldsymbol{c}_2 \\ \vdots \\ \boldsymbol{c}_\Theta \end{pmatrix},$$

which brings equation (3) into the form of equation (1):

$$\sum_{i=1}^{\Theta} \boldsymbol{S}_i \boldsymbol{c}_i = \begin{pmatrix} \boldsymbol{S}_1 & \boldsymbol{S}_2 & \dots & \boldsymbol{S}_\Theta \end{pmatrix} \begin{pmatrix} \boldsymbol{c}_1 \\ \boldsymbol{c}_2 \\ \vdots \\ \boldsymbol{c}_\Theta \end{pmatrix} = \tilde{\boldsymbol{S}}\tilde{\boldsymbol{c}} = \boldsymbol{u}. \tag{4}$$

For the solution of (4), again the Tikhonov regularized optimization approach

$$\tilde{\boldsymbol{c}}^* = \underset{\tilde{\boldsymbol{c}} \in \mathbb{R}_+^{\Theta N}}{\operatorname{argmin}} \|\tilde{\boldsymbol{S}}\tilde{\boldsymbol{c}} - \boldsymbol{u}\|_2^2 + \lambda \|\tilde{\boldsymbol{c}}\|_2^2 \tag{5}$$

is considered. The particle concentrations corresponding to the different samples, i.e. $\boldsymbol{c}_1, \boldsymbol{c}_2, \dots, \boldsymbol{c}_\Theta$ are extracted from the solution vector $\tilde{\boldsymbol{c}}^*$ and then can be visualized in separate images or blended into a single image using different colors. For both single- and multi-contrast MPI, we structurally end up at the same optimization problems as can be seen in equations (2) and (5).

3.2. Definition of channel leakage

Solving the standard single-contrast reconstruction problem (2) results in the solution $\boldsymbol{c}^*$ which is in practice the sum of the ground truth $\boldsymbol{c}$ and various artifact contributions. The solution $\boldsymbol{c}^*$ can be mathematically expressed as:

$$\boldsymbol{c}^* = \boldsymbol{c} + \boldsymbol{a}_c + \boldsymbol{a}_\eta, \tag{6}$$

where $\boldsymbol{a}_c$ represents the artifacts that are spatially correlated with the reconstructed object and is mostly dependent on the regularization method used. Such artifacts are commonly referred to as regularization bias, for example, an edge overshooting and blurring effect is obtained when applying the Tikhonov regularization model (Nawwas *et al* 2021). $\boldsymbol{a}_\eta$ denotes noise contributions that are not spatially correlated with the reconstructed object. The latter may vary significantly from frame to frame but are present regardless of the presence of an MPI tracer in the field of view (FOV).

In the multi-contrast setting, we analogously define

$$\tilde{\boldsymbol{c}}^* = \begin{pmatrix} \boldsymbol{c}_1^* \\ \\ \boldsymbol{c}_2^* \\ \\ \vdots \\ \\ \boldsymbol{c}_\Theta^* \end{pmatrix} = \begin{pmatrix} \boldsymbol{c}_1 + \boldsymbol{a}_{c_1} + \boldsymbol{a}_{\eta_1} + \sum\limits_{j \in \mathbb{J}/\{1\}} \boldsymbol{l}_{1,j} \\ \boldsymbol{c}_2 + \boldsymbol{a}_{c_2} + \boldsymbol{a}_{\eta_2} + \sum\limits_{j \in \mathbb{J}/\{2\}} \boldsymbol{l}_{2,j} \\ \vdots \\ \boldsymbol{c}_\Theta + \boldsymbol{a}_{c_\Theta} + \boldsymbol{a}_{\eta_\Theta} + \sum\limits_{j \in \mathbb{J}/\{\Theta\}} \boldsymbol{l}_{\Theta,j} \end{pmatrix}, \tag{7}$$

where $\mathbb{J} = \{1, 2, \dots, \Theta\}$, $\boldsymbol{a}_{c_i}$ and $\boldsymbol{a}_{\eta_i}, i \in \mathbb{J}$ are the corresponding artifacts just introduced for each channel *i*. Additionally, as indicated in section 2, $\boldsymbol{l}_{i,j}$ represents artifacts in channel *i* spatially correlated to the particle distribution $\boldsymbol{c}_j$ in channel *j*. We refer to these artifacts as leakage.

4. Materials and methods

4.1. Image reconstruction

Single- and multi-contrast image reconstruction requires solving optimization problems as defined in equation (5). Prior to reconstruction, measurements and system matrices are frequency filtered, i.e. a subset of frequency components I_{SNR} is selected for reconstruction by using a threshold σ on the signal-to-noise ratio (SNR) spectra of the frequency components

$$I_\sigma^{\boldsymbol{S}} = \{f_k \,|\, \text{SNR}(f_k) > \sigma\}, k \in \{1, \dots, M\}. \tag{8}$$

More details on the preparation steps of MPI problems reconstruction can be found in Scheffler *et al* (2024).

For the concatenated system matrix in multi-contrast MPI, commonly the intersection of the selected frequency components for each of the single system matrices is used, i.e.

$$I_\sigma^\cap = I_\sigma^{S_1} \cap I_\sigma^{S_2} \cap \ldots \cap I_\sigma^{S_\Theta}. \tag{9}$$

Frequency filtering is essential in MPI for reducing noise and is considered a regularization technique. For the sake of simplicity, we will keep on using the same notation for the system matrices before and after the frequency selection.

Equations (2) and (5) are solved using the row-based iterative linear solver, Kaczmarz, by applying it to the second normal equation (Hansen 1998), more details can be found in Knopp and Buzug (2012). Due to the physical properties of the particle concentration vector, a non-negativity constraint has to be included for it. For the MPI reconstruction and data processing, the Julia packages MPIReco.jl (Knopp *et al* 2019b) and MPIFiles.jl (Knopp *et al* 2019a) are used.

4.2. Two-step measurement & reconstruction method

The proposed two-step method for leakage reduction (Nawwas *et al* 2024b) uses modifications to both the measurement scheme and the reconstruction method. For the sake of simplicity, the method is explained for a two-channel multi-contrast model. The idea can be generalized to more channels. To start with the measurement scheme, this method introduces an extra prior measurement step where a single channel is measured with the other channel left empty as follows:

$$\begin{pmatrix} \boldsymbol{S}_1 & \boldsymbol{S}_2 \end{pmatrix} \begin{pmatrix} \hat{\boldsymbol{c}}_1 \\ \boldsymbol{0} \end{pmatrix} = \hat{\boldsymbol{u}}, \tag{10}$$

where $\boldsymbol{S}_1$ and $\boldsymbol{S}_2$ are the system matrices, $\hat{\boldsymbol{c}}_1$ is an approximation of the first channel phantom, and $\hat{\boldsymbol{u}}$ is the additional data measurement vector. This additional measurement data $\hat{\boldsymbol{u}}$ is exploited to quantify the leakage and thus reduce it. After that, the regular experiment measurement scheme is conducted, which can be formulated as

$$\begin{pmatrix} \boldsymbol{S}_1 & \boldsymbol{S}_2 \end{pmatrix} \begin{pmatrix} \boldsymbol{c}_1 \\ \boldsymbol{c}_2 \end{pmatrix} = \boldsymbol{u}, \tag{11}$$

where $\boldsymbol{c}_2$ represents the second channel phantom.

After reconstructing (11) using the Tikhonov regularized least-squares approach, we obtain the result

$$\begin{pmatrix} \boldsymbol{c}_1 + \boldsymbol{l}_{1,2} \\ \boldsymbol{c}_2 + \boldsymbol{l}_{2,1} \end{pmatrix}, \tag{12}$$

where $\boldsymbol{l}_{1,2}$ and $\boldsymbol{l}_{2,1}$ represent the leakage in the first and the second channel, respectively. Since channel leakage is the most dominant artifact contribution and the main focus of our work, we leave out the other artifact contributions discussed in section 3.2. Then we reconstruct (10) to get

$$\begin{pmatrix} \hat{\boldsymbol{c}}_1 \\ \hat{\boldsymbol{l}}_{2,1} \end{pmatrix}. \tag{13}$$

Assuming that $\boldsymbol{c}_1 \approx \hat{\boldsymbol{c}}_1$ and $\boldsymbol{l}_{2,1} \approx \hat{\boldsymbol{l}}_{2,1}$ and then subtracting (13) from (12) results in

$$\begin{pmatrix} (\boldsymbol{c}_1 + \boldsymbol{l}_{1,2}) - \hat{\boldsymbol{c}}_1 \\ (\boldsymbol{c}_2 + \boldsymbol{l}_{2,1}) - \hat{\boldsymbol{l}}_{2,1} \end{pmatrix} \approx \begin{pmatrix} \hat{\boldsymbol{l}}_{1,2} \\ \boldsymbol{c}_2 \end{pmatrix}, \tag{14}$$

where $\hat{\boldsymbol{l}}_{1,2}$ is an approximation of the leakage from the second channel and $\boldsymbol{c}_2$ is an approximation of the second channel phantom reconstruction with no leakage. In order to also remove the leakage from the first channel, we also assume that $\boldsymbol{l}_{1,2} \approx \hat{\boldsymbol{l}}_{1,2}$ and then subtract (14) from (12) to get

$$\begin{pmatrix} (\boldsymbol{c}_1 + \boldsymbol{l}_{1,2}) - \hat{\boldsymbol{l}}_{1,2} \\ (\boldsymbol{c}_2 + \boldsymbol{l}_{2,1}) - \boldsymbol{c}_2 \end{pmatrix} \approx \begin{pmatrix} \boldsymbol{c}_1 \\ \hat{\boldsymbol{l}}_{2,1} \end{pmatrix}, \tag{15}$$

where $\boldsymbol{c}_1$ is an approximation of the first channel phantom reconstruction with no leakage and $\hat{\boldsymbol{l}}_{2,1}$ is an approximation of the leakage from the first channel. Finally, sorting everything together, we get an approximation of a final solution with reduced leakage as follows

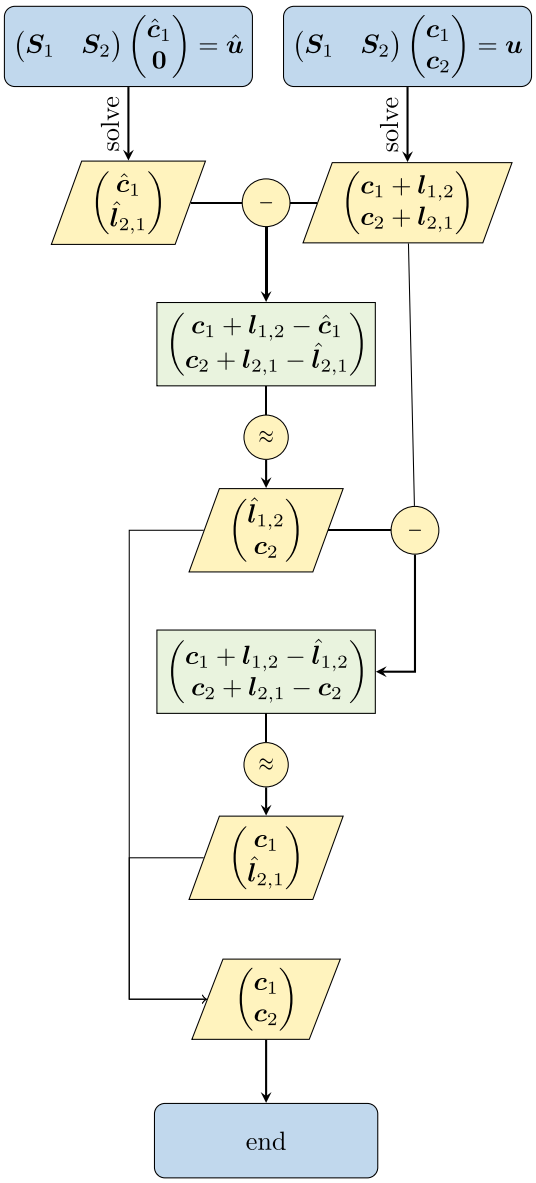

Figure 2. This flowchart shows the steps of the two-step reconstruction method for channel leakage reduction.

$$\begin{pmatrix}c_1\\c_2\end{pmatrix}.$$

The steps of our two-step reconstruction method are summed up in the following flowchart 2.

4.3. Simulation setup

A 2D simulation study is performed using two system matrices, both measured using a preclinical MPI system (Bruker, Ettlingen, Germany). For both system matrices, the drive field amplitudes were 12 mTμ_0^{-1} in x- and y-directions and the gradient strength was $G_x = G_y = -1$ Tm$^{-1}\mu_0^{-1}$ and $G_z = 2$ Tm$^{-1}\mu_0^{-1}$, which results in an effective FOV of 24×24 mm^2. The system matrices were measured on a 30×30 grid and a slightly larger area of 30×30 mm^2 which amounts to 7200 B of memory consumption per frequency component. The delta samples had a volume of $1 \times 1 \times 1$ mm^3. Both samples were filled with MPI tracer perimag (micromod Partikeltechnologie GmbH, Rostock, Germany); one with mobilized (liquid) perimag with a concentration of 0.5 mg$_{\text{Fe}}$ ml^{-1} and the other with immobilized (solid) perimag with a concentration of 1 mg$_{\text{Fe}}$ ml^{-1}. The acquisition time for each system matrix is approximately 15 min, based on the rule from Knopp *et al* (2017). For forward simulation, we used bicubically upsampled system matrices with an upsampling factor of 1.3 in each dimension to avoid committing an inverse crime, whereas unmodified system matrices are used for reconstruction.

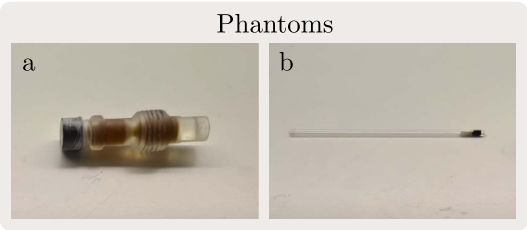

Figure 3. Pictures of the vessel stenosis phantom (a) and the catheter phantom (b) used in the experiment.

As an exemplary imaging experiment, we consider the scenario of catheter tracking in a vessel with stenosis. The catheter phantom is marked with the immobilized tracer at its tip and the vessel phantom is filled with the mobilized tracer. The following forward model is used to create the simulated data

$$\underbrace{\begin{pmatrix} \boldsymbol{S}_1 & \boldsymbol{S}_2 \end{pmatrix}}_{\boldsymbol{S}} \underbrace{\begin{pmatrix} \boldsymbol{c}_1 \\ \boldsymbol{c}_2 \end{pmatrix}}_{\boldsymbol{c}} + \boldsymbol{n} = \boldsymbol{u},$$

where $\boldsymbol{S}$ is the system matrix that consists of the mobilized ($\boldsymbol{S}_1$) and immobilized ($\boldsymbol{S}_2$) system matrices acquired for the two channels concatenated along the spatial axis, $\boldsymbol{u}$ is the measurement vector, and $\boldsymbol{n}$ is the white Gaussian noise vector with a variance of 0.5. The original phantoms used in the simulation are shown in the first row of figure 1, where $\boldsymbol{c}_1$ is the stenosis phantom and $\boldsymbol{c}_2$ is the catheter phantom. The two forward models (10) and (11) are used to create the needed simulated data sets, where the first considers keeping one of the channels empty and the other has the stenosis phantom as shown in the first image of figure 1 and the second considers having the stenosis and the catheter phantoms in the channels.

4.4. Experimental Setup

For our experimental study fluid and immobilized perimag filled system matrices, $\boldsymbol{S}_1$ and $\boldsymbol{S}_2$ are measured using a preclinical MPI scanner (Bruker, Ettlingen, Germany) on a grid of $24 \times 24 \times 24$. This amounts to a memory consumption of 108 KB per frequency component. The delta sample has a size of $2 \times 2 \times 1$ mm^3. The gradient field strength was 1.5 Tm$^{-1}\mu_0^{-1}$ in z-direction and -0.75 Tm$^{-1}\mu_0^{-1}$ in x- and y-direction. The drive field amplitude was 12 mTμ_0^{-1} in each direction. This created a FOV of size $18 \times 18 \times 9$ mm^3 and an approximated acquisition time of 4 hours (Knopp *et al* 2017).

A vessel stenosis phantom is 3D printed and then filled with perimag tracer as shown in figure 3(a). The vessel with stenosis phantom has a length of 40 mm, a maximum inner radius of 10 mm, a minimum inner radius of 5 mm, and a stenosis length of 4 mm. A thin glass capillary (outer diameter 1.7 mm/inner diameter 1.3 mm) is used as a catheter. The glass capillary is filled with a drop of perimag tracer and then mixed with an about equal amount of sodium alginate powder to immobilize the nanoparticles as seen in figure 3(b).

The following experiment is conducted while imaging. It starts with measuring the perimag-filled stenosis phantom alone with the other channel kept empty. Then, the thin glass capillary filled with a dot of immobilized perimag representing the catheter is introduced into the stenosis phantom and then moved through the FOV and back. The catheter movement is achieved via a custom-built inserting tool while the stenosis phantom is mounted along the scanner bore. This results in two different multi-contrast MPI datasets reconstructed from two measurements: the datasets of the catheter and the stenosis on the one hand, and the dataset of the stenosis and an empty channel on the other hand.

4.5. System matrix analysis

An analysis of the system matrices is performed to gain insights into the influence of the matrix concatenation in multi-contrast MPI on the system matrix properties, similar to what has been briefly introduced in Nawwas *et al* (2024a). Additionally, we investigate the influence of concatenation on the speed of convergence and the generation of channel leakage artifacts in multi-contrast reconstruction. The following points are considered:

4.5.1. Dimensionality

The convergence of the Kaczmarz method is significantly affected by the size of the linear system. While the method applies to overdetermined and underdetermined systems, its convergence behavior for overdetermined systems is better than for underdetermined systems (Xinyin *et al* 2020). Multi-contrast reconstruction requires concatenating the system matrices, which implies changing the dimensions of the

systems. This can affect the structure of the linear system, i.e. if it is overdetermined or underdetermined. The columns-to-rows ratio (CRR) is introduced as a measure for the dimensionality change in multi-contrast MPI. The CRR is the ratio of the number of columns to the number of rows in the linear system. A square linear system has a CRR of 1. If the CRR is less than 1, then the system is overdetermined and if it is greater than 1, then the system is underdetermined. The CRR is compared for the mobilized, immobilized, and concatenated system matrices for both the 2D simulation data and the 3D experimental data.

4.5.2. The condition number

The condition number of the system matrix $\boldsymbol{S}$, denoted as $\kappa(\boldsymbol{S})$, is given by the ratio of the largest and the smallest singular values. In general, the condition number of a matrix determines the stability and accuracy when solving a linear system. It also influences the convergence behavior of iterative linear solvers, such as the Kaczmarz method. A high condition number leads to slow convergence, while a low condition number results in fast convergence (Pyzara *et al* 2011). The condition numbers of the mobilized, immobilized, and concatenated system matrices in multi-contrast MPI are calculated and compared for both the 2D simulation data and the 3D experimental data.

4.5.3. Similarity of frequency components

When concatenating identical system matrices in multi-contrast MPI the reconstructed signal gets equally divided on all channels regardless of the phantoms existing in the channels, i.e. no signal separation is achieved in the channel dimension. Thus, it is essential to check the effect of the similarity between the corresponding frequency components for the concatenated system matrices on channel leakage. This is done by applying a second frequency filtering step to the multi-contrast system matrices based on the similarity of their frequency components. The NRMSD of the corresponding frequency components is used to evaluate their similarity as follows

$$\mathrm{NRMSD} = \frac{\mathrm{RMSD}}{\max_i\left(|\boldsymbol{S}_1^{i,\cdot}|\right) - \min_i\left(|\boldsymbol{S}_1^{i,\cdot}|\right)}, \tag{16}$$

$$\mathrm{RMSD} = \frac{\|\boldsymbol{S}_1^{i,\cdot} - \boldsymbol{S}_2^{i,\cdot}\|_2}{\sqrt{M}}, \tag{17}$$

where $\boldsymbol{S}_1^{i,\cdot}$ and $\boldsymbol{S}_2^{i,\cdot}$ are the ith rows of the system matrices $\boldsymbol{S}_1$ and $\boldsymbol{S}_2$, respectively. The concatenated system matrix is frequency-filtered in 3 different ways. First, using the commonly used SNR-threshold-based method, which is introduced in section 4.1. Different SNR thresholds are used, namely, 2, 4, 8, and 16. Second, the system matrix is first frequency filtered using an SNR threshold of 1, and then as a second frequency filtering step, the frequency components that show the highest similarity are selected. Third, the system matrix is first frequency filtered using an SNR threshold of 1 and then as a second frequency filtering step, the frequency components that show the lowest similarity are selected. Reconstructions are conducted using the resulting system matrices and the reconstruction results are visually compared.

4.6. Quantitative analysis

The quality of the reconstructed images is evaluated by first calculating the structural similarity (SSIM) index (Brooks *et al* 2008) for the simulated data, where the phantoms are available as ground truth. The SSIM index is calculated for each channel individually. SSIM measures the similarity of the reconstructed images to the real phantom, which makes it a good tool for image quality testing. The SSIM index is composed of three components: luminance, contrast, and structure. The relative importance of each of these components is controlled by some parameters, which are all equally weighted. The SSIM index is a real number between 0.0 and 1.0, and higher values of SSIM indicate higher image similarity. An SSIM index of 0.0 indicates a complete loss of all structural similarity while an SSIM index of 1.0 indicates having identical images.

To quantify the amount of leakage in the reconstructed images a leakage measure is introduced. It is motivated by the mathematical definition of leakage proposed in equation (7). A mask $\boldsymbol{m}_i, i = 1, \ldots, \Theta$ is created for each channel using an upscaled/extrapolated version of the channel's original phantom with the phantom pixels set to zeros and the rest set to ones. The mask is then applied to the reconstructed images and the mean of the non-zero pixels is summed up to represent the leakage per each channel as follows:

$$\mathfrak{L} = \frac{\sum_{i=1}^{\Theta} \boldsymbol{c}_i \,.\, \boldsymbol{m}_i}{N}. \tag{18}$$

This measure of leakage provides a more accurate approximation of the channel leakage as it becomes the dominant type of artifact.

5. Results

5.1. System matrix analysis

5.1.1. Dimensionality

Table 1 displays the CRR of the frequency-filtered mobilized, immobilized, and concatenated system matrices for both the 2D and 3D datasets. The table shows that the CRR of the concatenated system matrix is higher than the CRR of the mobilized, and immobilized system matrices. Thus, concatenating the system matrices for reconstruction in multi-contrast MPI significantly increases the underdetermination of the concatenated system.

5.1.2. The condition number

Table 2 lists the condition number of the mobilized, immobilized, and concatenated system matrices for both the 2D and 3D datasets. The table shows that the condition number of the joint system matrix is higher than it is for the single ones. This indicates that concatenating the system matrices in multi-contrast MPI leads to an increase in the condition number for the resulting joint system matrix.

5.1.3. Similarity of frequency components

Figure 4 shows the reconstruction results of the second channel, showing the catheter phantom, using different methods of frequency filtering. The parameter K represents the number of frequency components in the reconstruction. The first row displays reconstruction results using SNR-based frequency-filtered system matrices. The second row shows reconstruction results using the system matrices with high-similarity-frequency selection, and the third row uses the system matrices with low-similarity-frequency selection.

The reconstruction results obtained with the system matrices that include the most similar frequency components have the highest amount of leakage in the second channel, as shown in the second row. Reconstruction results in the third row show slightly less leakage into the second channel compared to the reconstructions in the first row. However, when using a small number of the frequency components for reconstruction, one notices more noise artifacts compared to the SNR-based frequency selection.

5.2. Two-step measurement method

5.2.1. Reconstruction results

Figure 5 displays the reconstruction results of the 2D simulated data presented in section 4.3 using the standard Kaczmarz method and the proposed two-step method for different numbers of iterations. For all reconstructions, the regularization parameter λ is relatively set to $1e-5$ using the L-curve method and for frequency filtering, an SNR threshold of 3 is used. The first two columns of figure 5 show the reconstruction results of the first measurement step of our method, where only the stenosis phantom is measured with the other channel empty. As can be seen, the first channel contains the reconstruction result of the stenosis phantom and the second channel shows the leakage from the first channel into the second one. It is also observed that the leakage artifacts in the second channel are spatially correlated with the stenosis phantom structure from the first channel, just as explained in section 3.2. One can also notice that the amount of leakage is reduced by applying more iterations of Kaczmarz. The third and fourth columns of the figure 5 show the reconstruction results of the second measurement step of our experiment where the catheter is inserted into the stenosis using the regular Kaczmarz method. The second channel displays the catheter phantom as well as the leakage signal from the first channel. With 10 Kaczmarz iterations, the leakage artifacts are significantly dominant making it hard to distinguish the catheter phantom in the second channel. With more Kaczmarz iterations, the leakage is reduced and the overall quality of the reconstructions is improved. The last two columns of figure 5 show the reconstruction results obtained using the proposed two-step reconstruction method. The second channel clearly shows the catheter phantom with almost no visible leakage even after only 10 Kaczmarz iterations. The reconstruction of the first channel phantom, the stenosis, is also visually improved as the leakage from the catheter phantom into the first channel is reduced.

Figure 6 shows the reconstruction results of the experimental 3D data using the standard Kaczmarz method and the proposed two-step method using 10 and 100 Kaczmarz iterations, a regularization parameter of $\lambda = 10^{-2}$, and an SNR threshold of 1.5 for frequency filtering. The regularization parameter λ is chosen based on the L-curve method. The first two columns show the reconstruction results of the first measurement step, where channel 1 shows the stenosis phantom and channel 2 shows the leakage from the

Table 1. The CRR of the system matrices before and after concatenation for both the 2D and 3D datasets is shown.

Columns to Rows Ratio (CRR)	2D	3D
Mobilized System Matrix	1.28	4.34
Immobilized System Matrix	1.28	4.34
Concatenated System Matrix	2.23	8.69

Table 2. The condition number of the system matrices before and after concatenation for both the 2D and 3D datasets is shown.

Condition Number	2D	3D
Mobilized System Matrix	$5.1.10^5$	$3.8.10^5$
Immobilized System Matrix	$8.2.10^5$	$3.8.10^5$
Concatenated System Matrix	$3.3.10^6$	$8.2.10^5$

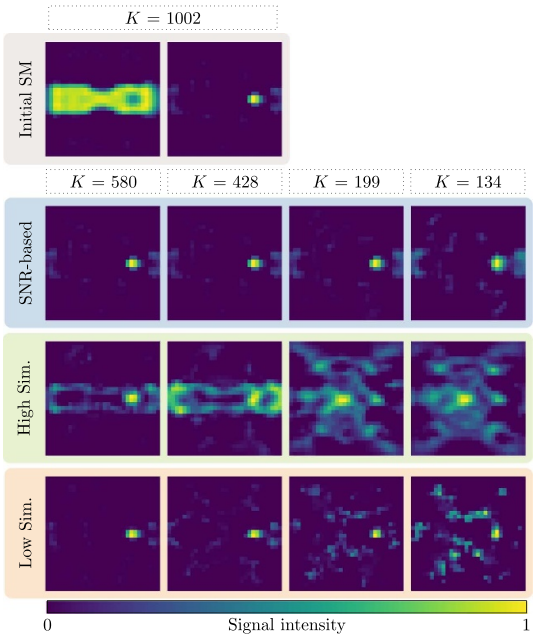

Figure 4. The reconstruction results of the second channel were obtained using system matrices with different frequency filtering methods. The first method was based on signal-to-noise ratio (SNR), the second on high similarity, and the third on low similarity.

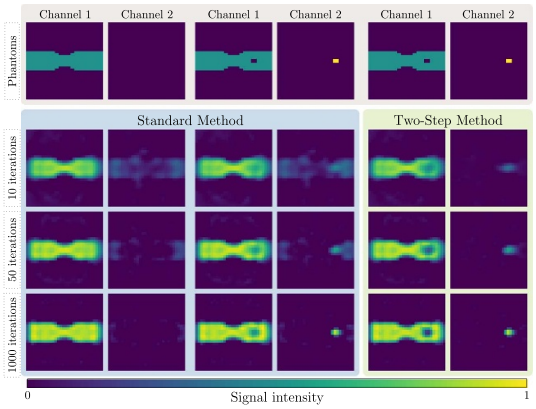

Figure 5. Reconstruction results of the 2D simulated data using the standard Kaczmarz method and the proposed two-step reconstruction method are shown for different numbers of iterations.

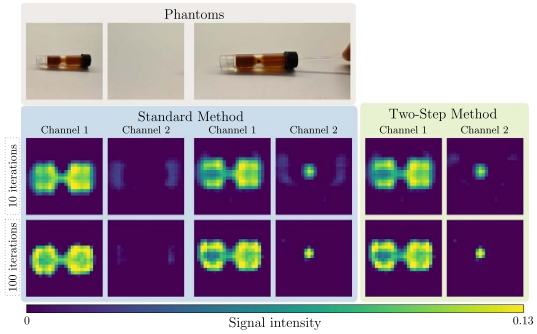

Figure 6. Reconstruction results of the 3D measured data are shown for the standard Kaczmarz method and the proposed two-step reconstruction method.

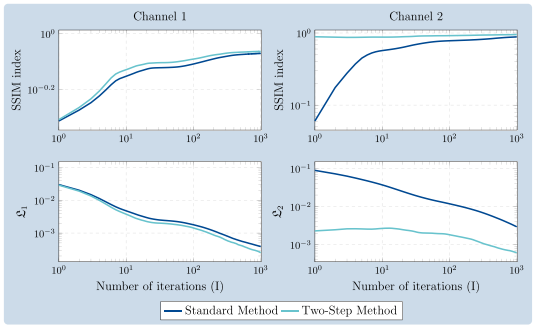

Figure 7. The SSIM index and the leakage are shown for both the standard Kaczmarz and the two-step method reconstructions along the number of iterations for channel 1 (left) and channel 2 (right).

first channel. The third and fourth columns show the reconstruction results of the second measurement step, where channel 1 and channel 2 show the stenosis and the catheter phantoms, respectively. It is noticed that with more Kaczmarz iterations, the leakage is reduced and the overall quality of the reconstructions is improved. The last two columns show the reconstruction results using our two-step method. This demonstrates that the leakage in channel 2 is significantly reduced using the two-step method.

The reconstruction results of both the simulated and the experimental datasets show similar observations of leakage reduction and convergence speedup using the proposed two-step method.

5.2.2. Leakage reduction evaluation

Figure 7 shows the SSIM index and the leakage metric (18) for the standard Kaczmarz and the two-step reconstruction methods versus the number of iterations for both channels of the simulated data. The SSIM index of the two-step method shows an overall improvement in the quality of the reconstructed images even with a small number of iterations, especially in the second channel. Comparing both channels, one can see that the improvement in the image quality when using the two-step method is more significant in the second channel.

From the leakage plot, it can first be observed that the amount of leakage decreases with an increasing number of Kaczmarz iterations. It also shows a reduction in the amount of leakage when using the two-step method, especially in the second channel as it suffers from more leakage artifacts. The leakage plot shows that the second channel generally has more leakage signal than the first one, which might be explained by the stronger signal in the first channel containing the fluid particles. Comparing both channels, it is also visible that the two-step method reduces the leakage in the second channel more than in the first one.

6. Discussion

The present work proposed a classification of commonly observed single- and multi-contrast MPI artifacts. Sources of these artifacts are analyzed with a special focus on multi-contrast specific channel leakage artifacts. Additionally, a measure to quantify channel leakage is introduced. Finally, a two-step measurement and reconstruction method aimed at the reduction of leakage is proposed. Its effectiveness is assessed using

simulated and experimental data considering an interventional imaging scenario. The proposed leakage-reduction method helped to reduce the leakage and improve the overall quality of the reconstruction. The leakage measure and the SSIM index are used to evaluate the effectiveness of the proposed method.

Most artifact types in MPI are shared between the single- and multi-contrast case, except for the channel leakage. Although it is possible on a theoretical level to classify types and sources of reconstruction artifacts, it is not always possible to visually attribute and distinguish the often overlapping artifacts for real MPI images. However, the classification of reconstruction artifacts and their sources helps in finding methods to reduce them. For example, the MPI reconstruction noise artifacts have a random structure and are not spatially correlated to the reconstructed object and they exist even when there are no tracers in the reconstructed FOV. Those noise artifacts are commonly reduced in MPI by applying tailored regularization (Storath *et al* 2017), frequency filtering (Knopp *et al* 2010), and other methods (Weber *et al* 2015). Channel leakage manifests as ghost-like artifacts in the shape of tracer distributions corresponding to other channels. It is an exclusive kind of artifact for multi-contrast MPI problems. In some cases, the channel leakage is so dominant that it severely affects the overall quality of the reconstruction and makes it difficult to distinguish individual structures.

This study investigated how the properties of multi-contrast system matrices affect the formation of leakage and convergence speed of the algebraic reconstruction. Concatenating the system matrices for reconstruction in multi-contrast MPI increases the underdetermination of the concatenated system and the severity of the increase is dependent on the number of channels being reconstructed in the application. The more channels, the more challenging the reconstruction is. The concatenation of the system matrices also increases the condition number of the concatenated system significantly. This increase in the underdetermination and the condition number of the concatenated system slows down the convergence of the iterative Kaczmarz solver for multi-contrast MPI reconstruction. Therefore, the number of Kaczmarz iterations needed for convergence increases from less than 10 for single-contrast MPI to up to 10 000 for multi-contrast MPI as observed in these applications (Möddel *et al* 2018, Shasha *et al* 2019).

The analysis of frequency filtering based on similarity shows that selecting high-similarity frequency components results in increased leakage while selecting low-similarity components results in decreased leakage. Therefore, the similarity of the frequency components of the system matrices in multi-contrast MPI plays a crucial role in the amount of leakage generated in the different channels. The more similar the frequency components of the concatenated system matrices are, the higher the generated leakage in the reconstructed images. Although this paper presents the results of only two datasets, the observations made on other multi-contrast datasets are consistent with the observations made here. The implications are that there is an interesting design space in the field of tracer synthesis to develop multi-contrast specific tracers that are easier to distinguish. In our specific case, we used the same particle once in a fluid and once in an immobilized state, the latter blocking the Brownian rotation. For Néel rotation-dominated tracers, maximizing the difference in particle signal could be achieved by changing the particle diameter and anisotropy. Here, one has to be careful since another important design criterion is the general signal strength, which implies that a trade-off needs to be made.

In this work, we propose a two-step method to reduce leakage that includes a specific measurement scheme and reconstruction method. The measurement scheme requires a pre-measurement step for the sake of leakage quantification and the reconstruction method provides estimates for the leakage, which are subtracted from the reconstruction. Thus, the limitation of the method comes from the feasibility of generally deriving applicable methods for leakage quantification. The catheter tracking in a vessel scenario introduced in this work shows a significant visual reduction of the leakage artifacts in the reconstruction results for both the simulated and the experimental datasets. The SSIM index and the leakage measure indicate that to obtain satisfactory reconstruction results with minimal channel leakage artifacts using the regular Kaczmarz solver, a high number of 1000 iterations is required. However, using the two-step method, similar results can be achieved with only 10 iterations. When using the proposed method, improvements in both the SSIM index and the leakage measure are observed for both channels. The improvements are more significant in the second channel where more severe leakage artifacts are present. In summary, the proposed method allows performing multi-contrast MPI reconstructions with a number of Kaczmarz iterations in the same order of magnitude as for single-contrast MPI.

Note that our proposed method is still limited to specific applications due to the feasibility of the leakage quantification step. Having measurements where only a single tracer is in the FOV, which remains rather static is not possible for all multi-contrast applications. Thus, investigating if our method can handle more multi-contrast applications by deriving new methods for leakage quantification would be beneficial for the method's improvement.

7. Conclusion

In summary, it has been shown that channel leakage artifacts are significant in multi-contrast MPI, slowing down the convergence of system matrix-based reconstruction and affecting the overall quality of the resulting images. The severity of these artifacts depends on the similarity of the corresponding frequency components and several other properties of the multi-patch system matrix, such as its shape and condition number, which we have studied and analyzed in detail. Our research also suggests that a frequency selection technique based on the similarity of the frequency components of the concatenated system matrices could significantly reduce channel leakage and accelerate convergence for multi-contrast MPI reconstructions. This should be investigated further in future work. The proposed leakage reduction technique has been shown to significantly reduce this problem and, as a result, multi-contrast MPI reconstructions can be performed with a similar number of Kaczmarz iterations as is the case for single-contrast MPI reconstructions. Thus, it makes multi-contrast MPI feasible for real-time imaging, removing a serious limitation.

Data availability statement

All data that support the findings of this study are included within the article (and any supplementary information files).

Acknowledgment

We gratefully acknowledge the assistance of Marija Boberg by sharing her insights to improve the manuscript.

ORCID iDs

Lina Nawwas https://orcid.org/0000-0002-1986-5229
Martin Möddel https://orcid.org/0000-0002-4737-7863
Tobias Knopp https://orcid.org/0000-0002-1589-8517

References

Barnhart R K and Steinmetz S 1999 Chambers dictionary of etymology *Mobius* (available at: https://books.google.co.uk/books?id=hwUB898kQmUC)
Barrett J F and Keat N 2004 Artifacts in CT: recognition and avoidance *RadioGraphics* **24** 1679–91
Bell D, Fahrenhorst-Jones T, Davtyan L 2018 Radiological image artifact (available at: https://radiopaedia.org/articles/61068)
Boas E and Fleischmann D 2012 CT artifacts: causes and reduction techniques *Imaging Med.* **4** 229–40
Brinkmann E, Burger M, Rasch J and Sutour C 2017 Bias reduction in variational regularization *J. Math. Imaging Vis.* **59** 534–66
Brooks A C, Zhao X and Pappas T N 2008 Structural similarity quality metrics in a coding context: Exploring the space of realistic distortions *IEEE Trans. Image Process.* **17** 1261–73
Budrys T, Veikutis V, Lukosevicius S, Gleizniene R, Monastyreckiene E and Kulakiene I 2018 Artifacts in magnetic resonance imaging: How it can really affect diagnostic image quality and confuse clinical diagnosis? *J. Vibroeng.* **20** 1202–13
Dietrich O, Reiser M F and Schoenberg S O 2008 Artifacts in 3-T MRI: Physical background and reduction strategies *Eur. J. Radiol.* **65** 29–35
Gleich B and Weizenecker J 2005 Tomographic imaging using the nonlinear response of magnetic particles *Nature* **435** 1214–7
Glöckner I, Möddel M, Knopp T and Brandt C 2020 Tailored regularization methods for multi-contrast magnetic particle imaging *Int. J. Magn. Part. Imaging* **6** 1–3
Grüttner M, Knopp T, Franke J, Heidenreich M, Rahmer J, Halkola A, Kaethner C, Borgert J and Buzug T M 2013 On the formulation of the image reconstruction problem in magnetic particle imaging *Biomed. Tech./Biomed. Eng.* **58** 583–91
Hansen P C 1998 *Rank-Deficient and Discrete Ill-Posed Problems* (SIAM)
Herbst M and Franke J 2018 Ghost correction for multi-parameter MPI *Book of Abstracts: 8th International Workshop on Magnetic Particle Imaging* ed T Knopp and T Buzug (Infinite Science Publishing) pp 67–68
Hsieh J 2009 *Computed Tomography: Principles, Design, Artifacts and Recent Advances.* (SPIE Digital Library)
Kluth T 2018 Mathematical models for magnetic particle imaging *Inverse Problems* **34** 083001
Knopp T and Buzug T 2012 *Magnetic Particle Imaging: An Introduction to Imaging Principles and Scanner Instrumentation* (Springer)
Knopp T, Gdaniec N and Möddel M 2017 Magnetic particle imaging: from proof of principle to preclinical applications *Phys. Med. Biol.* **62** R124
Knopp T, Möddel M, Griese F, Werner F, Szwargulski P and Gdaniec N 2019a MPIFiles.jl: A julia package for magnetic particle imaging files *J. Open Source Softw.* **4** 1331
Knopp T, Rahmer J, Sattel T F, Biederer S, Weizenecker J, Gleich B, Borgert J and Buzug T M 2010 Weighted iterative reconstruction for magnetic particle imaging *Phys. Med. Biol.* **55** 1577–89
Knopp T, Szwargulski P, Griese F, Grosser M, Boberg M and Möddel M 2019b MPIReco.jl: Julia package for image reconstruction in mpi *Int. J. Magn. Part. Imaging* **5**
Möddel M, Griese F, Kluth T and Knopp T 2021 Estimating the spatial orientation of immobilized magnetic nanoparticles with parallel-aligned easy axes *Phys. Rev. Appl.* **16** L041003

Möddel M, Meins C, Dieckhoff J and Knopp T 2018 Viscosity quantification using multi-contrast magnetic particle imaging *New J. Phys.* **20** 083001
Mori I, Machida Y and Osanai M 2013 Photon starvation artifacts of x-ray CT: their true cause and a solution *Radiol. Phys. Technol.* **6** 130–41
Nawwas L, Brandt C, Szwargulski P, Knopp T and Möddel M 2021 Reduction of bias for sparsity promoting regularization in MPI *Int. J. Magn. Part. Imaging* **7** 1–3
Nawwas L, Möddel M and Knopp T 2024a Influence of the system matrix on channel leakage artifacts in multi-contrast MPI *Int. J. Magn. Part. Imaging* **10** 1–4
Nawwas L, Möddel M and Knopp T 2024b Multi-contrast MPI channel leakage reduction using a two-step measurement and reconstruction method *Int. J. Magn. Part. Imaging* **10** 1–4
Pyzara A, Bylina B and Bylina J 2011 The influence of a matrix condition number on iterative methods' convergence pp 459–64
Rahmer J, Halkola A, Gleich B, Schmale I and Borgert J 2015 First experimental evidence of the feasibility of multi-color magnetic particle imaging *Phys. Med. Biol.* **60** 1775
Scheffler K, Boberg M and Knopp T 2024 Solving the MPI reconstruction problem with automatically tuned regularization parameters *Phys. Med. Biol.* **69** 045024
Shasha C, Teeman E, Krishnan K M, Szwargulski P, Knopp T and Möddel M 2019 Discriminating nanoparticle core size using multi-contrast MPI *Phys. Med. Biol.* **64** 074001
Shetty C M, Barthur A, Kambadakone A, Narayanan N and Kv R 2011 Computed radiography image artifacts revisited *Am. J. Roentgenol.* **196** W37–W47
Stehning C, Gleich B and Rahmer J 2016 Simultaneous magnetic particle imaging (MPI) and temperature mapping using multi-color MPI *Int. J. Magn. Part. Imaging* **2**
Storath M, Brandt C, Hofmann M, Knopp T, Salamon J, Weber A and Weinmann A 2017 Edge preserving and noise reducing reconstruction for magnetic particle imaging *IEEE Trans. Med. Imaging* **36** 74–85
Triche B L, Nelson J T, McGill N S, Porter K K, Sanyal R, Tessler F N, McConathy J E, Gauntt D M, Yester M V and Singh S P 2019 Recognizing and minimizing artifacts at CT, MRI, US and Molecular imaging *RadioGraphics* **39** 1017–8
Walz-Flannigan A, Magnuson D, Erickson D and Schueler B 2012 Artifacts in digital radiography *Am. J. Roentgenol.* **198** 156–61
Weber A, Werner F, Weizenecker J, Buzug T M and Knopp T 2015 Artifact-free reconstruction with the system matrix approach by overscanning the field-free-point trajectory in magnetic particle imaging *Phys. Med. Biol.* **61** 475
Xinyin H, Gang L and Qiang N 2020 *Remarks on Kaczmarz Algorithm for Solving Consistent and Inconsistent System of Linear Equations* vol 12138 (Springer)